



# Nitrogen-doped carbon dots as a ratiometric fluorescent probe for determination of the activity of acid phosphatase, for inhibitor screening, and for intracellular imaging

Zhenmao Zhu<sup>1</sup> · Xiaoyun Lin<sup>1</sup> · Lina Wu<sup>1</sup> · Chengfei Zhao<sup>1</sup> · Shaoguang Li<sup>1</sup> · Ailin Liu<sup>1</sup> · Xinhua Lin<sup>1,2</sup> · Liqing Lin<sup>1,2</sup>

Received: 10 January 2019 / Accepted: 12 June 2019 / Published online: 23 July 2019  
© Springer-Verlag GmbH Austria, part of Springer Nature 2019

## Abstract

The authors describe a method for preparation of green fluorescent nitrogen-doped carbon dots (N-CDs) through hydrothermal treatment of a mixture of lotus leaf juice and ethylenediamine (EDA). The N-CDs have uniform size, good dispersibility and water solubility. Under 316 and 366 nm photoexcitation, they show dual fluorescence with emission peaks at 415 and 509 nm, respectively. They are positively charged and display low cytotoxicity. This makes them an excellent choice for fluorometric assays and for bioimaging. A ratiometric assay was developed for the determination of the activity of acid phosphatase (ACP). It is based on the aggregation-induced quenching (AIQ) of the fluorescence of the N-CDs by sodium hexametaphosphate ( $\text{NaPO}_3$ )<sub>6</sub>. Enzymatic hydrolysis of ( $\text{NaPO}_3$ )<sub>6</sub> by ACP leads to the disintegration of ( $\text{NaPO}_3$ )<sub>6</sub> and to the restoration of fluorescence. The measurement of the ratio of fluorescence at two wavelengths (415 and 509 nm), background interference and fluctuating signals can be widely eliminated. The method works in the 1–50 U·L<sup>-1</sup> ACP activity range and has a detection limit of 0.43 U·L<sup>-1</sup>. It was successfully applied (a) to the determination of ACP in spiked serum samples, (b) to ACP inhibitor screening, and (c) to imaging of ACP in HePG2 cells.

**Keywords** Fluorescence · Lotus leaf · Ethylenediamine · Sodium hexametaphosphate · Aggregation-induced quenching · Electrostatic interactions · Enzymatic hydrolysis · ACP inhibitor

## Introduction

Acid phosphatase (ACP) is a hydrolase that catalyzes the hydrolysis of orthophosphate monoester to form inorganic phosphate under acidic conditions [1]. It is widespread in nature and can be found in a variety of animal and plant species [2]. It

is found that an abnormal elevated level of ACP in the human body indicates the pathophysiological process of several diseases including Gaucher disease [3], hyperparathyroidism [4], metastasized prostate cancer [5], multiple myeloma [6] and et al. Clinically, accurate monitoring of ACP level in blood has been used for the medical diagnosis and drug screening of related diseases. That is because ACP is always recognized as an important serum marker, a useful prognostic indicator and can be used as a drug target [7, 8]. Therefore, the development of reliable and sensitive ACP assays is of great clinical significance, especially in the diagnosis of human prostatic diseases and prostatic cancer.

A number of assays for ACP has been reported, including immunoassay [9], electrochemical [10], performance liquid chromatography [11], fluorescence spectrophotometry methods [12] and colorimetric [13]. Among these methods, fluorometric assay is considered as the more desirable method due to its high sensitivity, convenience, real-time, accessible instrument requirement and does not require highly trained operators [14]. However, most of

---

Zhenmao Zhu and Xiaoyun Lin contributed equally to this work.

**Electronic supplementary material** The online version of this article (<https://doi.org/10.1007/s00604-019-3600-9>) contains supplementary material, which is available to authorized users.

✉ Liqing Lin  
fjmu\_lin@126.com

<sup>1</sup> Department of Pharmaceutical Analysis, School of Pharmacy, Fujian Medical University, Fuzhou 350108, People's Republic of China

<sup>2</sup> Higher Educational Key Laboratory for Nano Biomedical Technology of Fujian Province, Fujian Medical University, Fuzhou 350004, People's Republic of China

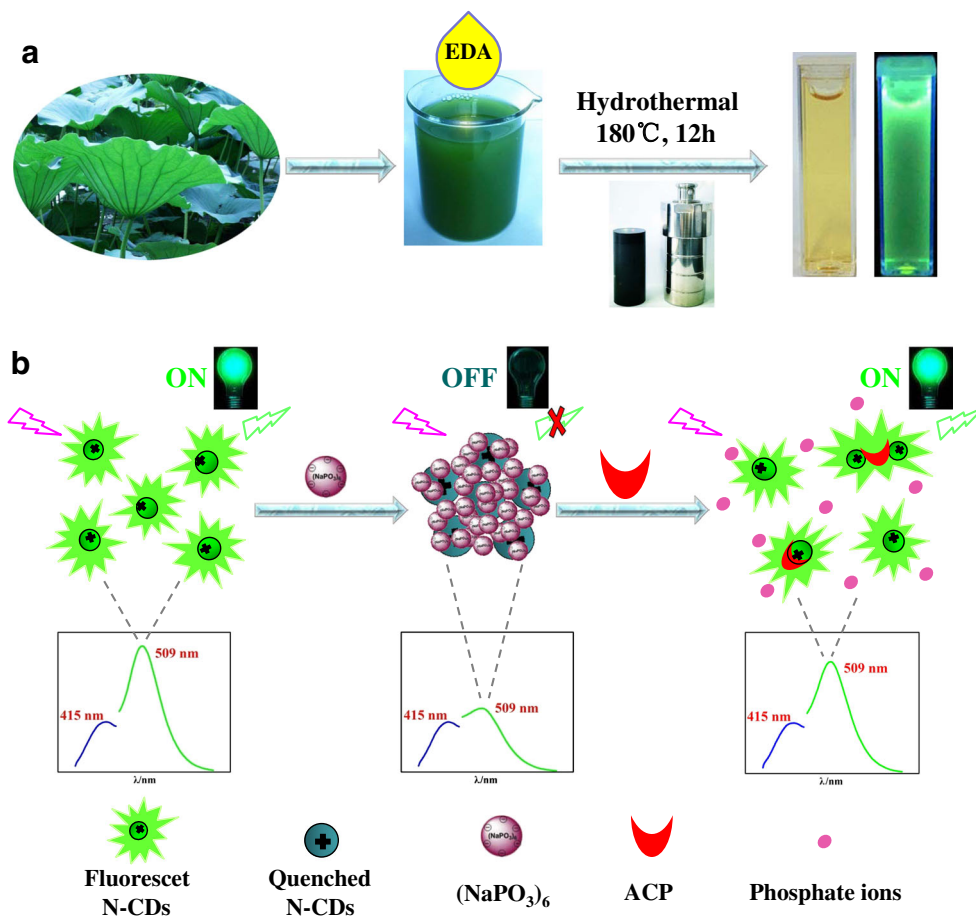
fluorometric assays for ACP are focused on fluorescence “turn-off” [12, 15–17]. The applications of these methods are limited due to their higher false-positive responses and lower selectivity [18]. In addition, whether it is a fluorescence “turn-on” or “turn-off” model, such a solely responsive signal is readily perturbed by various factors associated with instrument and environment, and thus prevented their further practical applications [19]. Ratiometric fluorescence can largely minimize the possible interfering effects both arising from instrument and environment through recording the ratio of fluorescence intensities at two different wavelengths. Compared with single-signal steady-state fluorescence, ratiometric fluorescence technique could achieve more accurate and effective detection, which makes it more suitable for the practical applications [20].

Carbon dots (CDs) have drawn considerable attention in the applications for bioimaging, fluorescent sensing, drug delivery, photocatalysis, optoelectronic devices, etc. [21–23]. Compared to toxic metal-based semiconductor quantum dots and organic dyes fluorescent probes, CDs have the advantages of higher aqueous solubility, easier surface functionalization, higher resistance to photobleaching, lower toxicity and better biocompatibility

[24, 25]. These excellent properties make CDs a promising benign fluorescent nanomaterial. Among numerous CDs synthesis methods [26], one-pot hydrothermal carbonization of natural biomass to provide CDs is an attractive route, not only because of the facile and eco-friendly reaction process, but also the cheap and sustainable raw materials [27]. For practical applications, especially in the case of biomedicine, it is highly desirable to use green raw materials to synthesize long wavelength emissive CDs through environmentally friendly reaction pathways.

We present an economical and eco-friendly approach to prepare green fluorescent biomass N-CDs by one-pot hydrothermal carbonization using lotus leaf juice and EDA as the carbon precursor and nitrogen source, respectively (Scheme 1a). The N-CDs are positively charged and have double unique fluorescence emission peaks. On this basis, an efficient ratiometric fluorescent probe for ACP activity detection has been performed. In aqueous buffer of appropriate pH, N-CDs are positively charged and have highly fluorescence, while there are six negative charges in  $(\text{NaPO}_3)_6$ . Therefore, the N-CDs favor to form aggregate assembly with  $(\text{NaPO}_3)_6$  via strong attractive electrostatic interactions. Scheme 1b shows that the 509 nm fluorescence is quenched by  $(\text{NaPO}_3)_6$  via the AIQ. The 415 nm fluorescence, in

**Scheme 1** Schematic illustration of (a) the preparation of N-CDs from lotus leaf, (b) the design and principle for ACP detection based on the AIQ and enzymolysis approach.



contrast, remains almost unchanged. In the presence of ACP, ACP can specifically hydrolyze  $(\text{NaPO}_3)_6$  into phosphate fragments, resulting in the destruction of the N-CDs/ $(\text{NaPO}_3)_6$  aggregation. Consequently, the quenched fluorescence at 509 nm is restored. So an efficient ratiometric fluorescent probe is developed with 509 nm fluorescence emission as the probe and 415 nm fluorescence emission as the internal reference for ACP detection. It is firstly that lotus-derived biomass N-CDs can be used to construct a ratiometric fluorescent probe for ACP assay. The method can be successfully applied for ACP determining in spiked serum samples, ACP inhibitor screening and intracellular ACP imaging.

## Experimental

Reagents and apparatus required for the experiment and some experimental steps are detailed in the Electronic Supporting Material (ESM).

### Synthesis of nitrogen-doped carbon dots (N-CDs)

N-CDs were synthesized according to previously reported procedure with a certain modification [27]. Lotus leaf juice and EDA were selected as the carbon precursor and nitrogen

source, respectively. The detailed synthesis steps are shown in the ESM (Table S1, Fig. S1, S2, S3).

### Acid phosphatase (ACP) detection

In a typical assay, 150  $\mu\text{L}$  acetate buffer (10 mM, pH = 4.8), 10  $\mu\text{L}$  N-CDs ( $1 \text{ mg}\cdot\text{mL}^{-1}$ ) and 20  $\mu\text{L}$   $(\text{NaPO}_3)_6$  solution (3 mM) successively added into 0.5 mL calibrated test tubes, then mixed thoroughly at room temperature. Subsequently, 20  $\mu\text{L}$  different activities of ACP standard solution (diluted with 10 mM, pH = 4.8, acetate buffer) were added into the above mixtures. Then, these samples were incubated in 37 °C bath for 2 h. After incubation, the fluorescence intensity of the mixtures was measured at 415 and 509 nm with excitation at 366 nm.

### The inhibition effect of $\text{Na}_2\text{MoO}_4$

20  $\mu\text{L}$   $(\text{NaPO}_3)_6$  (3 mM), 20  $\mu\text{L}$  ACP ( $600 \text{ U}\cdot\text{L}^{-1}$ ) and 20  $\mu\text{L}$  different concentrations of  $\text{Na}_2\text{MoO}_4$  were incubated in 37 °C bath for 2 h. Then, 130  $\mu\text{L}$  acetate buffer (10 mM, pH = 4.8) and 10  $\mu\text{L}$  N-CDs ( $1 \text{ mg}\cdot\text{mL}^{-1}$ ) were added into the above reaction mixture and followed by recording the fluorescence spectrum of each solution. The inhibition efficiency (IE%) of  $\text{Na}_2\text{MoO}_4$  was calculated by the following equation:

$$\text{Inhibition Efficiency (IE\%)} = \frac{(\Delta F_{509\text{nm}}/F_{415\text{nm}})_{\text{no inhibitor}} - (\Delta F_{509\text{nm}}/F_{415\text{nm}})_{\text{inhibitor}}}{(\Delta F_{509\text{nm}}/F_{415\text{nm}})_{\text{no inhibitor}}} \times 100\%$$

Where  $(\Delta F_{509\text{nm}}/F_{415\text{nm}})_{\text{no inhibitor}}$  and  $(\Delta F_{509\text{nm}}/F_{415\text{nm}})_{\text{inhibitor}}$  are the fluorescence ratio of N-CDs/ $(\text{NaPO}_3)_6$ /ACP system in the absence and presence of  $\text{Na}_2\text{MoO}_4$ , respectively.  $\Delta F_{509\text{nm}}$  stands for the fluorescence difference of the system in the absence and presence of ACP.  $F_{415\text{nm}}$  is the fluorescence intensity at 415 nm excited by 366 nm. The half-maximal inhibition value (IC<sub>50</sub>) was obtained from the plot of inhibition efficiency of  $\text{Na}_2\text{MoO}_4$  as a function of its concentration.

### In vitro cell imaging

Human hepatoma cells HePG2 were seeded into a six-well plate at a density of  $6 \times 10^4$  cells per well and cultured in RPMI 1640 medium supplemented with 10% fetal bovine serum and 1% penicillin-streptomycin in an incubator (37 °C, 5% CO<sub>2</sub>) for 24 h. Then, the medium was removed and the adherent cells were washed with phosphate buffer saline (PBS) three times. Subsequently, a certain amount of ACP was added to the HePG2 cell wells. After incubation for 2 h, free ACP was removed from ACP-uptaken HePG2 cells by washing three times with PBS. Afterwards, 1 mL reaction

solution (PBS:RPMI 1640 = 4:1, pH = 4.8) containing 50  $\mu\text{g}\cdot\text{mL}^{-1}$  N-CDs and 300  $\mu\text{M}$   $(\text{NaPO}_3)_6$  was introduced into chambers with an incubation time of 2 h. Prior to imaging, removed the solution, and then washed cells with PBS for three times. The bright field and fluorescent images of cells were obtained on inverted fluorescence microscope.

## Results and discussion

### Choice of materials

The use of biomass to prepare CDs is attractive because it is green, cheap and can be used for large-scale preparation. More importantly, since the raw material comes from natural biomass, the CDs exhibit excellent biocompatibility, which is particularly suitable for bio-applications [28]. Lotus, an extensively cultivated aquatic plant in eastern Asia, is usually waste product of the lotus industry and easy to get. Lotus leaf-derived biomass N-CDs have unique double fluorescence emission peaks and emit green fluorescence. This makes them

an excellent choice for fluorometric assays and for bioimaging.

### Characterization and properties investigation of N-CDs

CDs were characterized by XPS, FT-IR spectroscopy and zeta potential, respectively (Fig. S4). XPS analysis suggests that the CDs consist of carbon, nitrogen and oxygen. Combining the analytical results of XPS and FT-IR, we deduced that the CDs are N-CDs, and have the predominant functional groups, including the hydroxyl, carbonyl group and amine group. Zeta potential measurements indicate that N-CDs are positively charged in the pH range of 0–8.6. The detail characterization for CDs is presented in ESM.

The morphological characteristics of the N-CDs were investigated by transmission electron microscopy (TEM). As shown in Fig. 1a, the monodispersed N-CDs have a uniform size with an average diameter of  $2.92 \pm 0.30$  nm (Fig. 1b).

This result is well supported by the dynamic light scattering spectra (Fig. S5a). The high-resolution TEM (HRTEM) image (inset of Fig. 1a (a)) reveals the high crystallinity of the N-CDs. The lattice spacing of 0.21 nm agrees with that of in-plane lattice spacing of graphene (100 facet) [29]. In addition, N-CDs exhibit excellent water-solubility (inset of Fig. 1a (b)).

The optical properties of the N-CDs were studied by UV-vis spectroscopy and fluorescence spectroscopy. As shown in Fig. 1c, N-CDs show two absorption peaks at 290 and 350 nm, which correspond to the  $\pi$ - $\pi^*$  transition of aromatic  $sp^2$  domains and  $n$ - $\pi^*$  transition of C=O, respectively [14]. In aqueous solution, N-CDs exhibit a luminescence wavelength maximum at 509 nm with 366 nm excitation (Fig. 1c), resulting in a strong green photoluminescence under 365 nm UV lamp (the inset in Fig. 1c). To further investigate the photoluminescent properties of the N-CDs, we carried out a detailed fluorescence study with different excitation wavelengths. As shown in Fig. 1d, the fluorescence emission spectra show unusual emission peaks. When the excitation

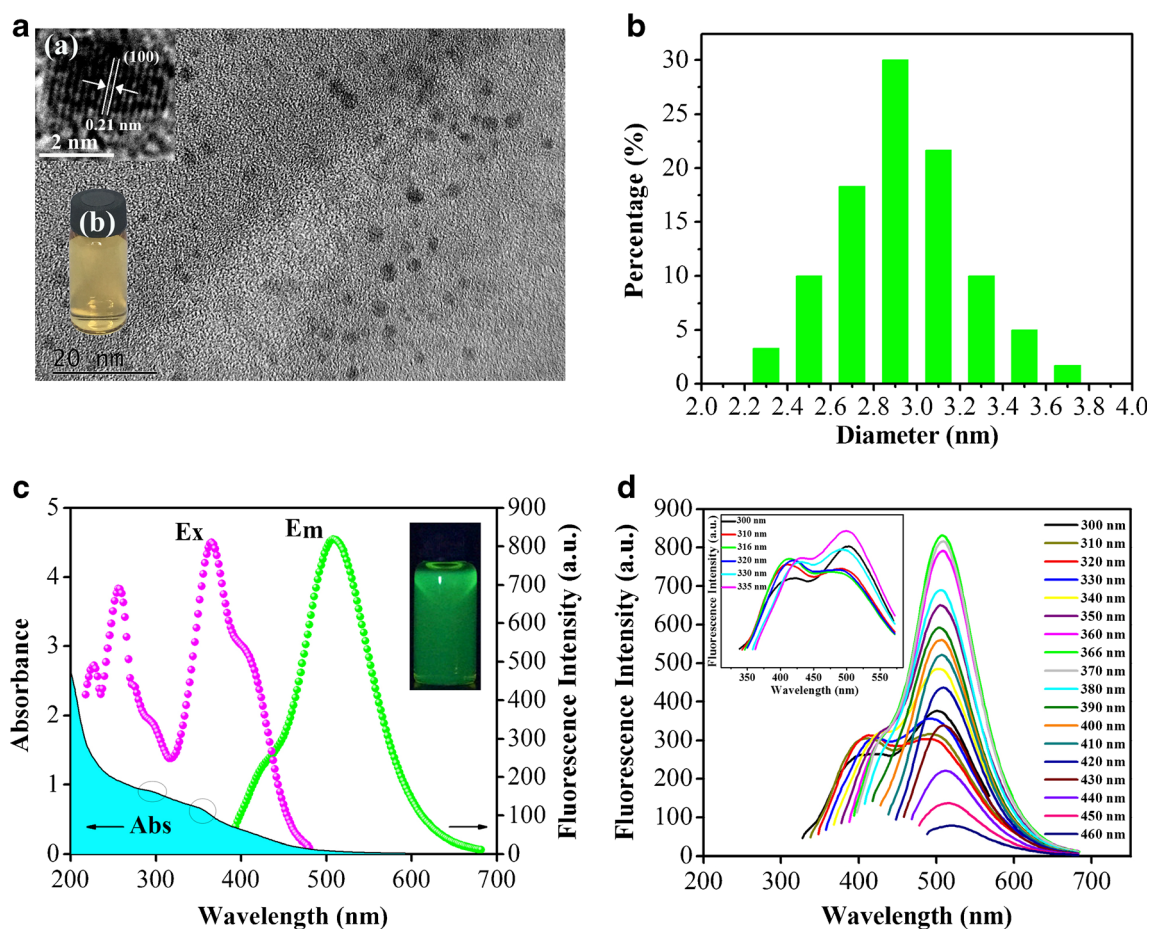


**Fig. 1** **a** TEM image of N-CDs. Inset: ((a)) high resolution TEM image of N-CDs; ((b)) photograph of N-CDs aqueous solution. **b** Size distribution of N-CDs. **c** UV-vis absorption, photoluminescence excitation ( $\lambda_{ex} = 366$  nm) and emission ( $\lambda_{em} = 509$  nm) spectra of N-CDs aqueous

solution. Inset shows the photograph of N-CDs aqueous solution under 365 nm UV lamp. **d** Fluorescence emission spectra of N-CDs under excitation wavelengths from 300 to 460 nm

wavelength ranges from 300 to 335 nm, the fluorescence emission spectra show two obviously emission peaks (inset of Fig. 1d), in which the optimal excitation wavelength of the first emission peak is 316 nm (Fig. S6). These two emission peaks are assigned to the band gap luminescence and defect luminescence, respectively [30]. Interestingly, the first fluorescence emission peak, which is located at a position of about 415 nm, gradually disappeared with the red-shift of the excitation wavelength, and the emission spectra show only one peak around 509 nm. This unique double emission peak makes it possible to design a ratiometric fluorescent probe. Moreover, the quantum yield (QY) of the N-CDs is calculated to be 8.6% using quinine sulfate as reference (Fig. S7), which is higher than that of undoped CDs (4.6%). Furthermore, the N-CDs aqueous solutions have excellent salt stability, pH stability and optical stability (Fig. S8, S9).

Since low toxicity is crucial for a variety of practical biological applications, the cytotoxicity of N-CDs was assessed by HepG2 cells using the standard MTT cell viability assay. Fig. S10 shows the viability of HepG2 cells incubated with different concentrations of N-CDs for different time. More than 91% cells can survive after incubation with N-CDs even at concentrations of  $400 \mu\text{g}\cdot\text{mL}^{-1}$  for 24 h, indicating the very low cytotoxicity of N-CDs. The excellent water solubility, stable fluorescence and low cytotoxicity of the N-CDs promised the cell imaging application.

## The detection strategy and principle of the ACP assay

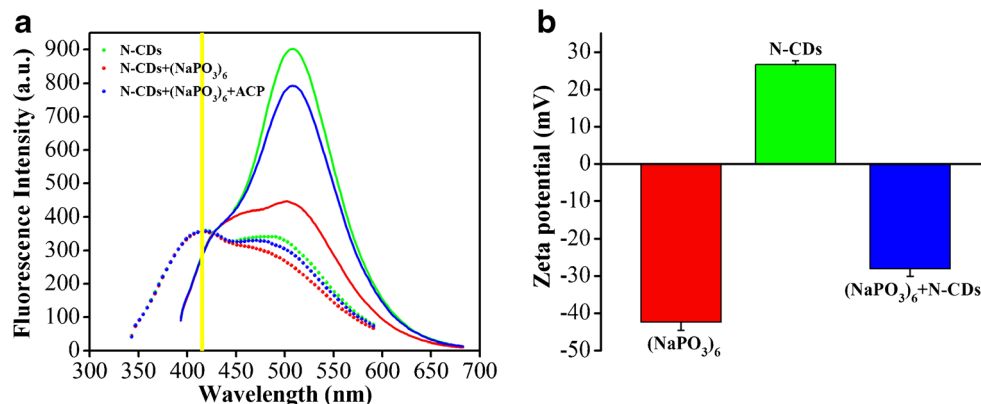
The fluorescence emission spectra of N-CDs, N-CDs/ $(\text{NaPO}_3)_6$  and N-CDs/ $(\text{NaPO}_3)_6$ /ACP are shown in Fig. 2a. It can be seen that the original emission peak fluorescence intensity of N-CDs located near 509 nm can be effectively quenched by the addition of  $(\text{NaPO}_3)_6$  regardless of whether it is excited by 316 nm or 366 nm. Moreover, the fluorescence intensity of system is significantly recovered in the presence of ACP. However, as for the first peak, the fluorescence intensity of N-CDs at 415 nm does not change with the addition of  $(\text{NaPO}_3)_6$  or  $(\text{NaPO}_3)_6$ /ACP when excited at 316 nm.

Simultaneously, we find that when excited at 366 nm, the fluorescence intensity of N-CDs in the range of 400 to 430 nm does not change with the reaction process, although there is no obvious peak shape near 415 nm. For simplicity and efficiency, single-wavelength excitation is the pursuit of ratiometric fluorescent probe. Therefore, a ratiometric fluorescent probe with 366 nm as the single excitation wavelength and fluorescence intensity at 415 nm as the internal reference is proposed for ACP activity detection.

To better understand the quenching process, a series of experiments were performed. As shown in Fig. S5a, the particle diameter of the N-CDs is about 2.88 nm. After adding  $(\text{NaPO}_3)_6$ , the particle diameter increases to 19.73 nm (Fig. S5b), and keeps substantially unchanged within 5 h (Fig. S5c). The zeta potential of  $(\text{NaPO}_3)_6$ , N-CDs and N-CDs/ $(\text{NaPO}_3)_6$  are shown in Fig. 2b. It can be seen that  $(\text{NaPO}_3)_6$  is negatively charged ( $\zeta = -42.37$  mV) while the N-CDs are positively charged ( $\zeta = +26.60$  mV). After mixed of N-CDs and  $(\text{NaPO}_3)_6$ , the zeta potential of system is  $-28.03$  mV. These results indicate that the high quenching efficiency is due to the fact that the positively charged N-CDs are non-covalently bonded to the negatively charged  $(\text{NaPO}_3)_6$  by electrostatic interaction to form a N-CDs/ $(\text{NaPO}_3)_6$  complex. At the same time, the initial strong fluorescence of the dispersive N-CDs has a dramatically decrease due to the AIQ property [31, 32]. In addition, other phosphate esters, such as ATP, AAP and PPI were selected as the quenchers. However, due to limited negative charge, the desired results have not been achieved (Fig. S11) [33].

To further reveal the detection mechanism of ACP, the time-resolved fluorescence decay of the N-CDs before and after the addition of  $(\text{NaPO}_3)_6$  or the further addition of ACP were also compared. As shown in Fig. S12, the calculated average lifetime value of N-CDs is around of 16.18 ns, which decreases to 13.63 ns after reacting with  $(\text{NaPO}_3)_6$ . The reduced lifetime reveals that the quenching mechanism is due to the ultrafast electron-transfer process between N-CDs and  $(\text{NaPO}_3)_6$  [34], which is a dynamic quenching mechanism. The lifetime of N-CDs increases to 15.29 ns with further

**Fig. 2** **a** Fluorescence emission spectra of N-CDs (green line), N-CDs/ $(\text{NaPO}_3)_6$  (red line), N-CDs/ $(\text{NaPO}_3)_6$ /ACP (blue line). The solid and dashed lines are the emission spectra under excitation of 366 nm and 316 nm, respectively. **b** The zeta potential of  $(\text{NaPO}_3)_6$ , N-CDs and N-CDs/ $(\text{NaPO}_3)_6$  mixture in the acetate buffer (10 mM, pH = 4.8)



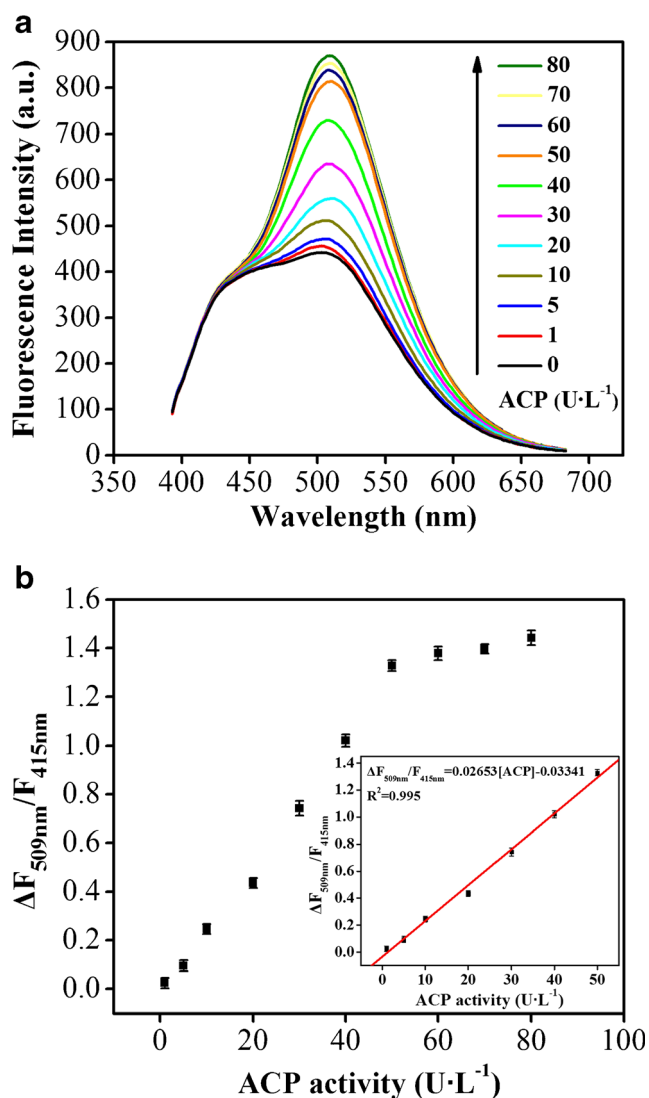
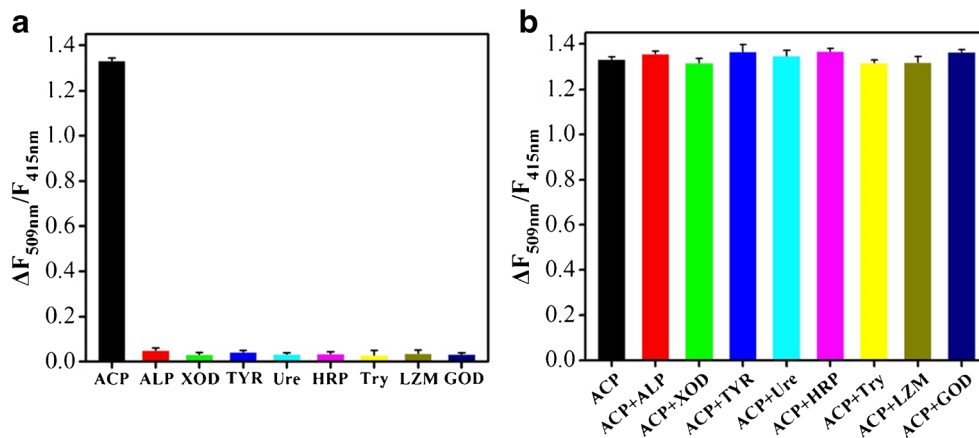


**Fig. 3** **a** Fluorescence emission spectra of N-CDs/(NaPO<sub>3</sub>)<sub>6</sub> system in the presence of different activities of ACP. **b** The relationship between  $\Delta F_{509\text{nm}}/F_{415\text{nm}}$  and the activity of ACP. The inset shows the linear plot of  $\Delta F_{509\text{nm}}/F_{415\text{nm}}$  against the activity of ACP, in which  $\Delta F_{509\text{nm}}$  is the change of fluorescence intensity at 509 nm before and after ACP is added into the N-CDs/(NaPO<sub>3</sub>)<sub>6</sub> system, and  $F_{415\text{nm}}$  is the fluorescence intensity at 415 nm with the excitation of 366 nm

**Fig. 4** **a**  $\Delta F_{509\text{nm}}/F_{415\text{nm}}$  of the N-CDs/(NaPO<sub>3</sub>)<sub>6</sub> system in the presence of interfering substances. **b**  $\Delta F_{509\text{nm}}/F_{415\text{nm}}$  of the N-CDs/(NaPO<sub>3</sub>)<sub>6</sub>/ACP system in the presence of interfering substances. The activity of ACP is 50 U·L<sup>-1</sup>, and the others are 1000 U·L<sup>-1</sup>



addition of ACP, which indicates that ACP can disassociate (NaPO<sub>3</sub>)<sub>6</sub> from N-CDs through enzymatic hydrolysis action.

### Optimization of method

The following parameters were optimized: (a) pH of solution; (b) Concentration of (NaPO<sub>3</sub>)<sub>6</sub>; (c) Reaction temperature; (d) Reaction time. Respective text and figures on optimizations are given in the ESM (Fig. S13, S14). In short, the following experimental conditions are found to give best results: (a) Best solution pH value is 4.8; (b) Best concentration of (NaPO<sub>3</sub>)<sub>6</sub> is 300 μM; (c) Best reaction temperature is 37 °C; (d) Best reaction time is 2 h.

### Sensitive and selective detection of ACP

Under the optimum conditions, the fluorescence emission spectra of the system upon the addition of different activities of ACP were recorded. From Fig. 3a, we can see the fluorescence intensity at 509 nm increases gradually with the increasing activity of ACP, while the fluorescence intensity at 415 nm is almost unchanged. The ratio of  $\Delta F_{509\text{nm}}/F_{415\text{nm}}$  is employed in the quantitative analysis of ACP, and a typical plot of the  $\Delta F_{509\text{nm}}/F_{415\text{nm}}$  versus ACP activity (1–80 U·L<sup>-1</sup>) is shown in Fig. 3b. Furthermore, a good linear relationship between  $\Delta F_{509\text{nm}}/F_{415\text{nm}}$  and the activity of ACP within the range of 1–50 U·L<sup>-1</sup> is plotted in the inset of Fig. 3b. The linear regression equation is  $\Delta F_{509\text{nm}}/F_{415\text{nm}} = 0.02653[\text{ACP}] - 0.03341$  with a correlation coefficient  $R^2$  of 0.995, and the limit detection is evaluated to be 0.43 U·L<sup>-1</sup> (S/N=3). As shown in Fig. S15, the relative standard deviation (RSD) is 2.5% for 32 U·L<sup>-1</sup> ACP ( $n=30$ ), indicating that the reproducibility and reliability of the method is satisfactory. It exhibits comparable sensitivity and lower RSD comparing with other reported detection methods shown in Table S2. It has been reported that the normal level of ACP in blood serum is 35–123 U·L<sup>-1</sup> [35]. Thus, the method satisfies the detection requirements for ACP quantification.

To demonstrate the specificity of the ratiometric fluorescent probe for ACP detection, the detection system was treated

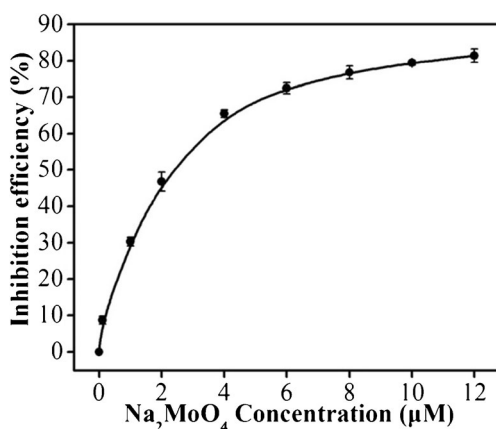


**Fig. 5** ACP inhibition efficiency of Na<sub>2</sub>MoO<sub>4</sub>. The data shown in the figures represent the average of three independent experiments ( $n = 3$ )

with several enzymes including alkaline phosphatase (ALP), xanthine oxidase (XOD), tyrosinase (TYR), urease (Ure), horseradish peroxidase (HRP), trypsin (Try), lysozyme (LZM) and glucose oxidase (GOD) under the same conditions. As shown in Fig. 4a, the fluorescence intensity of the N-CDs/(NaPO<sub>3</sub>)<sub>6</sub> system changes significantly with the addition of ACP, whereas other enzymes at an activity 20 times higher than that of ACP exhibits negligible effects. In addition, the anti-interference performance of the ratiometric fluorescent probe was also evaluated (Fig. 4b). The result shows that  $\Delta F_{509nm}/F_{415nm}$  is very close in the presence and absence of interfering substances. Furthermore, common ions and

small molecules also do not produce an obvious signal (Fig. S16). These results substantially indicate that the ratiometric fluorescent probe has a high selectivity toward ACP.

### Determination of ACP in human serum samples

In order to evaluate the practicality of the ratiometric fluorescent probe, the real sample assay was conducted using three different human serum samples and the detail presents in ESM. As shown in Table S3, we can see that the recoveries of ACP in the spiked samples range from 96.02% to 103.79% and the RSD values are no more than 3.54%, indicating that the ratiometric fluorescent probe is appropriate for ACP analysis in real samples.

### ACP inhibitor screening

Considering the hydrolysis of (NaPO<sub>3</sub>)<sub>6</sub> by ACP can be affected in the presence of the corresponding ACP inhibitors, our method can also be used for the screening of potential ACP inhibitors. In this work, Na<sub>2</sub>MoO<sub>4</sub>, a typical inhibitor of ACP, was employed as a model inhibitor to demonstrate the ability for this application. As shown in Fig. 5, with increasing concentrations of Na<sub>2</sub>MoO<sub>4</sub>, the IE% constantly increases, and the IC<sub>50</sub> value of Na<sub>2</sub>MoO<sub>4</sub> is calculated to be 2.018 µM. This result clearly indicated that our method can be utilized for the screening of potential ACP inhibitors.

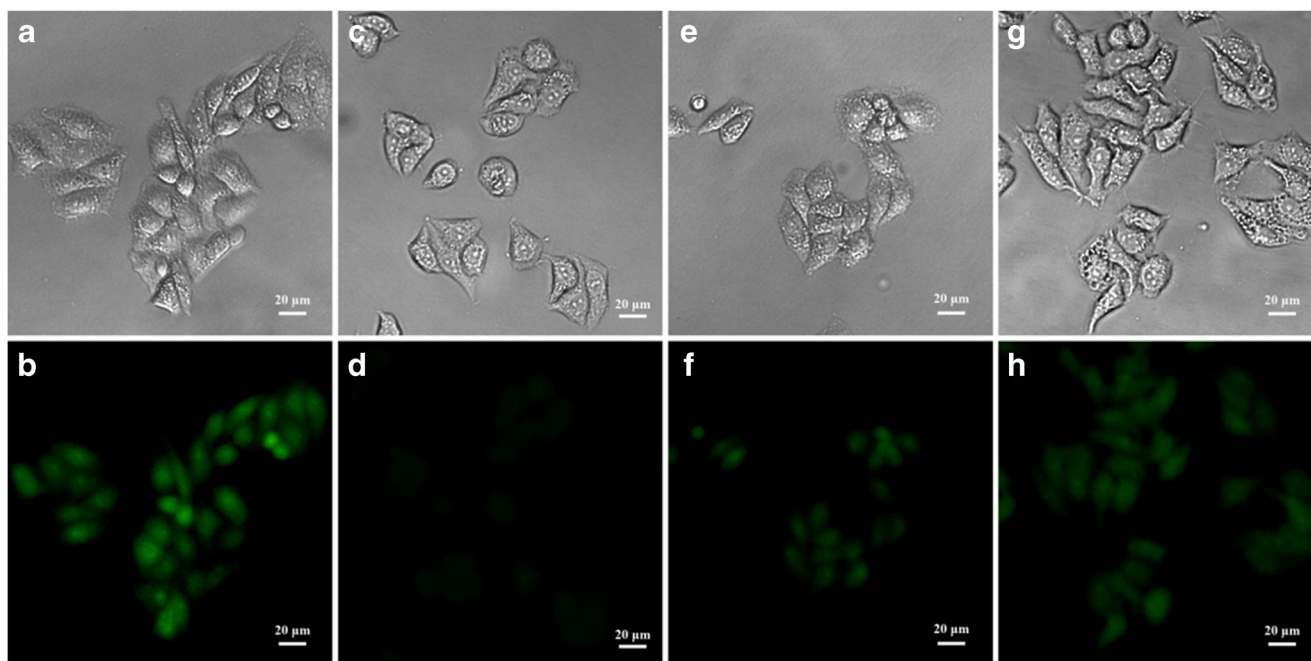


**Fig. 6** The bright field and fluorescent microscopy images of HepG2 cells incubated with 50 µg·mL<sup>-1</sup> N-CDs (a and b), non-ACP-uptaken HepG2 cells incubated with 50 µg·mL<sup>-1</sup> N-CDs and 300 µM (NaPO<sub>3</sub>)<sub>6</sub> (c and d), 50 U·L<sup>-1</sup>-ACP-uptaken HepG2 cells incubated with

50 µg·mL<sup>-1</sup> N-CDs and 300 µM (NaPO<sub>3</sub>)<sub>6</sub> (e and f), 100 U·L<sup>-1</sup>-ACP-uptaken HepG2 cells incubated with 50 µg·mL<sup>-1</sup> N-CDs and 300 µM (NaPO<sub>3</sub>)<sub>6</sub> (g and h) with excitation at 488 nm

## In vitro study

In order to evaluate the potential of the N-CDs/(NaPO<sub>3</sub>)<sub>6</sub> system for bioimaging applications, we further used the probe for intracellular ACP imaging in HepG2 cells by the standard addition method. As shown in Fig. 6b, after the incubation of N-CDs with HepG2 cells for 2 h, the fluorescence microscopic image shows strong intracellular green fluorescence signal of N-CDs. From Fig. 6d, we can see the green fluorescence significantly decreases in the intracellular when the N-CDs/(NaPO<sub>3</sub>)<sub>6</sub> is incubated with non-ACP-uptaken HepG2 cells. In contrast, there is a recovery of intracellular fluorescence in the ACP (50 U·L<sup>-1</sup>)-uptaken HepG2 cells with N-CDs/(NaPO<sub>3</sub>)<sub>6</sub> (Fig. 6f). Furthermore, the cells exposed to 100 U·L<sup>-1</sup> of ACP display stronger green fluorescence (Fig. 6h) than those exposed to 50 U·L<sup>-1</sup> of ACP. The fluorescence change between Fig. 6d, f and h clearly shows that our method can be potentially used for ACP activity detection in the intracellular region.

It should be noted that this work has certain limitations. Lotus is a seasonal plant that is not available at certain time of the year, which may lead to a shortage of raw materials. In addition, since the biomatter always display strong background UV absorption and fluorescence, the UV light used for fluorescence excitation will be screened off and this will weaken the signal. In this study, dried lotus leaves are also proved to be suitable for N-CDs synthesis, which solves the problem of raw material supply to some extent (Fig. S2, S3). The human serum samples used are subjected to a certain pre-treatment, the interference of serum albumin can be eliminated and the recovery can be improved. Thus, the method possesses high potential for practical applications.

## Conclusions

We have synthesized N-CDs by one-pot hydrothermal carbonization of lotus leaf juice and EDA. Since the raw material comes from natural biomass, the N-CDs exhibit excellent biocompatibility, which is particularly suitable for bio-applications. In addition, the N-CDs have unique dual fluorescence emission peaks and do not require external introduction of fluorophores, which avoids cumbersome introductions. A ratiometric fluorescent probe is presented for ACP detection based on the use of the N-CDs. By utilizing the  $\Delta F_{509\text{nm}}/F_{415\text{nm}}$  as the signal readout, the possible interfering effects both arising from instrument and environment are largely minimized, ensuring more reliable results. It should be noted that this work has certain limitations. For samples with complex components, some pre-treatments are required to eliminate interference and improve recovery. Since the method is well selective, sensitive and repeatable, it will provide a potential

platform for ACP determination in clinical diagnosis and ACP inhibitor screening in drug discovery.

**Acknowledgements** The authors gratefully acknowledge the financial support of the National Natural Science Foundation of China (21775023, 81703477), the Natural Science Foundation of Fujian Province (2016 J01368), Joint Funds for the Innovation of Science and Technology, Fujian Province (2016Y9055, 2017Y9124).

**Compliance with ethical standards** The author(s) declare that they have no competing interests.

## References

- Xie YH, Tan Y, Liu RX, Zhao R, Tan CY, Jiang YY (2012) Continuous and sensitive acid phosphatase assay based on a conjugated polyelectrolyte. *ACS Appl Mater Interfaces* 4:3784–3787
- Lin ZH, Liu ZP, Zhang H, Su XG (2015) Near-infrared fluorescence probe for the determination of acid phosphatase and imaging of prostate cancer cells. *Analyst* 140:1629–1636
- Tuchman LR, Swick M (1957) High acid phosphatase level indicating Gaucher's disease in patient with prostatism. *JAMA* 164:2034–2035
- Yam LT (1974) Clinical significance of the human acid phosphatases: a review. *Am J Med* 56:604–616
- Wang RH, Cai QY, Tong DF, Nie LH, Yao SZ (1998) Enzymatic assay of acid phosphatase and microanalysis of Cu<sup>2+</sup> and Ag<sup>+</sup> with a SAW-impedance sensor. *Enzym Microb Technol* 22:36–41
- Terpos E, de la Fuente J, Szydlo R, Hatjiharissi E, Viniou N, Meletis J, Yataganas X, Goldman JM, Rahemtulla A (2003) Tartrate-resistant acid phosphatase isoform 5b: a novel serum marker for monitoring bone disease in multiple myeloma. *Int J Cancer* 106:455–457
- Makarov DV, Loeb S, Getzenberg RH, Partin AW (2009) Biomarkers for prostate Cancer. *Annu Rev Med* 60:139–151
- Huang YY, Feng H, Liu WD, Zhou YY, Tang C, Ao H, Zhao MZ, Chen GL, Chen JR, Qian ZS (2016) Luminescent aggregated copper nanoclusters nanoswitch controlled by hydrophobic interaction for real-time monitoring of acid phosphatase activity. *Anal Chem* 88:11575–11583
- Stanley CJ, Cox RB, Cardosi MF, Turner APF (1988) Amperometric enzyme-amplified immunoassays. *J Immunol Methods* 112:153–161
- Calvo-Marzal P, Rosatto SS, Granjeiro PA, Aoyama H, Kubota LT (2001) Electroanalytical determination of acid phosphatase activity by monitoring p-nitrophenol. *Anal Chim Acta* 441:207–214
- Yamauchi Y, Ido M, Maeda H (2005) High performance liquid chromatography equipped with a cathodic detector and column-switching device as a high-throughput method for a phosphatase assay with p-nitrophenyl phosphate. *J Chromatogr A* 1066:127–132
- Qian ZS, Chai LJ, Zhou Q, Huang YY, Tang C, Chen JR, Feng H (2015) Reversible fluorescent nanoswitch based on carbon quantum dots nanoassembly for real-time acid phosphatase activity monitoring. *Anal Chem* 87:7332–7339
- Deng HH, Lin XL, Liu YH, Li KL, Zhuang QQ, Peng HP, Liu AL, Xia XH, Chen W (2017) Chitosan-stabilized platinum nanoparticles as effective oxidase mimics for colorimetric detection of acid phosphatase. *Nanoscale* 9:10292–10300
- Zhu ZM, Lin XY, Wu LN, Zhao CF, Zheng YJ, Liu AL, Lin LQ, Lin XH (2018) "Switch-on" fluorescent nanosensor based on nitrogen-doped carbon dots-MnO<sub>2</sub> nanocomposites for probing the activity of acid phosphatase. *Sensors Actuators B Chem* 274:609–615



15. Shi FP, Zhang Y, Na WD, Zhang XY, Li Y, Su XG (2016) Graphene quantum dots as selective fluorescence sensor for the detection of ascorbic acid and acid phosphatase via Cr(VI)/Cr(III)-modulated redox reaction. *J Mater Chem B* 4:3278–3285
16. Wang J, Yan Y, Yan X, Hu TY, Tang XJ, Su XG (2016) Label-free fluorescent assay for high sensitivity and selectivity detection of acid phosphatase and inhibitor screening. *Sensor Actuat B: Chem* 234:470–477
17. Yan X, Hu TY, Wang L, Zhang LN, Su XG (2016) Near-infrared fluorescence nanoprobe for enzyme-substrate system sensing and in vitro imaging. *Biosens Bioelectron* 79:922–929
18. Zhuang Y, Xu Q, Huang FJ, Gao PC, Zhao ZJ, Lou XD, Xia F (2016) Ratiometric fluorescent bioprobe for highly reproducible detection of telomerase in bloody urines of bladder cancer patients. *ACS Sensors* 5:572–578
19. Zhang ZZ, Wu YM, He SZ, Xu YY, Li GP, Ye BX (2018) Ratiometric fluorescence sensing of mercuric ion based on dye-doped lanthanide coordination polymer particles. *Anal Chim Acta* 1014:85–90
20. Fan DQ, Shang CS, Gu WL, Wang EK, Dong SJ (2017) Introducing ratiometric fluorescence to MnO<sub>2</sub> nanosheet-based biosensing: a simple, label-free ratiometric fluorescent sensor programmed by cascade logic circuit for ultrasensitive GSH detection. *ACS Appl Mater Interfaces* 9(31):25870–25877
21. Niu WJ, Li Y, Zhu RH, Shan D, Fan YR, Zhang XJ (2015) Ethylenediamine-assisted hydrothermal synthesis of nitrogen-doped carbon quantum dots as fluorescent probes for sensitive biosensing and bioimaging. *Sensors Actuators B Chem* 218:229–236
22. Zhang HJ, Chen YL, Liang MJ, Xu LF, Qi SD, Chen HL, Chen XG (2014) Solid-phase synthesis of highly fluorescent nitrogen-doped carbon dots for sensitive and selective probing ferric ions in living cells. *Anal Chem* 86:9846–9852
23. Tang M, Teng P, Long Y, Wang X, Liang L, Shen D, Wang J, Zheng H (2018) Hollow carbon dots labeled with FITC or TRITC for use in fluorescent cellular imaging. *Microchim Acta* 185:223–228
24. Yin BD, Deng JH, Peng X, Long Q, Zhao JG, Lu QJ, Chen Q, Li HT, Tang H, Zhang YY, Yao SZ (2013) Green synthesis of carbon dots with down-and up-conversion fluorescent properties for sensitive detection of hypochlorite with a dual-readout assay. *Analyst* 138:6551–6557
25. Wang R, Wang X, Sun Y (2017) Aminophenol-based carbon dots with dual wavelength fluorescence emission for determination of heparin. *Microchim Acta* 184:187–193
26. Zhou J, Zhou H, Tang J, Deng S, Yan F, Li WJ, Qu MH (2017) Carbon dots doped with heteroatoms for fluorescent bioimaging: a review. *Microchim Acta* 184:343–368
27. Liao J, Cheng ZH, Zhou L (2016) Nitrogen-doping enhanced fluorescent carbon dots: green synthesis and their applications for bioimaging and label-free detection of Au<sup>3+</sup> ions. *ACS Sustain Chem Eng* 4(6):3053–3061
28. Chen DX, Zhao JJ, Zhang LL, Liu RJ, Huang Y, Lan CQ, Zhao SL (2018) Capsicum-derived biomass quantum dots coupled with alizarin red S as an inner-filter-mediated illuminant Nanosystem for imaging of intracellular calcium ions. *Anal Chem* 90:13059–13064
29. Dong Y, Pang H, Yang HB, Guo C, Shao J, Chi Y, Li M, Yu T (2013) Carbon-based dots co-doped with nitrogen and sulfur for high quantum yield and excitation-independent emission. *Angew Chem* 125:7954–7958
30. Yang YM, Kong WQ, Li H, Liu J, Yang MM, Huang H, Liu Y, Wang ZY, Wang ZP, Sham TK, Zhong J, Wang C, Liu Z, Lee ST, Kang ZH (2015) Fluorescent N-doped carbon dots as in vitro and in vivo nanothermometer. *ACS Appl Mater Interfaces* 7(49):27324–27330
31. Huang BH, Geng ZR, Yan SH, Li Z, Cai J, Wang ZL (2017) Water-soluble conjugated polymer as a fluorescent probe for monitoring adenosine triphosphate level fluctuation in cell membranes during cell apoptosis and in vivo. *Anal Chem* 89:8816–8821
32. Xu YQ, Li BH, Xiao LL, Ouyang J, Sun SG, Pang Y (2014) A colorimetric and near-infrared fluorescent probe with high sensitivity and selectivity for acid phosphatase and inhibitor screening. *Chem Commun* 50:8677–8680
33. Guo P, Yan SY, Zhou YM, Wang CC, Xu XW, Weng XC, Zhou X (2013) A novel fluorescent “turn-off/turn-on” system for the detection of acid phosphatase activity. *Analyst* 138:3365–3367
34. Liu ZE, Xiao JC, Wu XW, Lin LQ, Weng SH, Chen M, Cai XH, Lin XH (2016) Switch-on fluorescent strategy based on N and S co-doped graphene quantum dots (N-S/GQDs) for monitoring pyrophosphate ions in synovial fluid of arthritis patients. *Sensors Actuators B Chem* 229:217–224
35. Hassan SSM, Sayour HEM, Kamel AH (2009) A simple-potentiometric method for determination of acid and alkaline phosphatase enzymes in biological fluids and dairy products using a nitrophenylphosphate plastic membrane sensor. *Anal Chim Acta* 640:75–81

**Publisher's note** Springer Nature remains neutral with regard to jurisdictional claims in published maps and institutional affiliations.